VIENNA UNIVERSITY OF TECHNOLOGY

FACULTY OF MECHANICAL AND INDUSTRIAL ENGINEERING

INSTITUTE OF LIGHTWEIGHT DESIGN AND STRUCTURAL BIOMECHANICS

COMPOSITE ENGINEERING

REPORT FROM TUTORIAL PART

EVALUATION OF THE EFFECTIVE MATERIAL PROPERTIES

2013/2014 WS

MICHAL ANDO

M.N.:1327785

Problem description:

The main goal of this work is to evaluate the material properties of uni-directional glass-epoxy composite. To estimate this properties, analytical and finite element approach were chosen.

Analytical approach represents the methods of Mori-Tanaka and Hashin-Shtrikman bounds. To compute required material properties, provided software for analytical computations (Compcomp) was used.

Finite element approach is based on periodic homogenization. Proper periodicity and symmetry boundary conditions were applied on the unit cell and sufficient number of independent material parameters were estimated. For this purpose was used a finite element software (Calculix).

Glass fibers and epoxy matrix are isotropic materials and their elastic and thermal material properties are shown in fig. 1. The fiber volume fraction is 0.4.

Glass			**Epoxy**		
Elastic modulus [GPa]	CTE [K^{-1}]	Poisson constant [-]	Elastic modulus [GPa]	CTE [K^{-1}]	Poisson constant [-]
80	$4.9\ 10^{-6}$	0.2	1.35	$130\ 10^{-6}$	0.3

Fig. 1. Material parameters of the glass-epoxy composite

Figure 2. represent examinated unit cell with its characteristic dimension and master nodes:

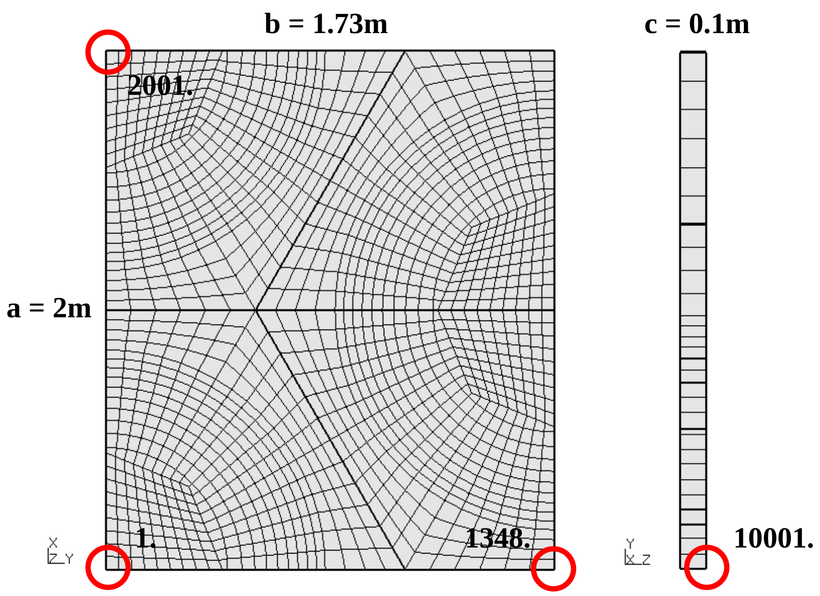

Fig. 2. Unit cell dimensions and master nodes

Longitudinal tension

Boundary conditions for master nodes are showed in the figure 3. Note that load is for every load case equal $F = 1767{,}5\ KN$.

Corresponding modulus	Master nodes	x-displacement [m]	y-displacement [m]	z-displacement [m]
E_l	1 (0,0,0)	FIXED	FIXED	FIXED
	1348 (0, 1.73,0)	FIXED	FREE	FIXED
	2001 (2,0,0)	FREE	FIXED	FIXED
	10001 (0,0, 0.1)	FREE	FREE	LOAD

Fig. 3. Boundary conditions for longitudinal tension

Master nodes displacements are showed in the figure 4.:

Corresponding modulus	Master nodes	x-displacement [m]	y-displacement [m]	z-displacement [m]
E_l	1 (0,0,0)	0	0	0
	1348 (0, 1.73,0)	0	-6.7850e-06	0
	2001 (2,0,0)	-7.8347e-06	0	0
	10001 (0,0, 0.1)	0	0	1.5549e-06

Fig. 4. Master nodes displacements for longitudinal tension

Computation of the longitudinal tension modulus:

$$\frac{F}{a \cdot b} = E_l \cdot \frac{z_{10001}}{c} \rightarrow E_l = \frac{c \cdot F}{a \cdot b \cdot z_{10001}} = \frac{0.1 \cdot 1{,}7675 \cdot e^{6}}{2 \cdot 1.73 \cdot 1.5549 \cdot \mathrm{e}^{-6}} = 3.2815 \cdot \mathrm{e}^{10}\ Pa$$

Computation of the longitudinal poisson ratio:

$$\nu_{tl} = -\frac{\varepsilon_{tt}}{\varepsilon_{ll}} = \frac{\frac{y_{1348}}{b}}{\frac{z_{10001}}{c}} = -\frac{\frac{-6.7850 \cdot \mathrm{e}^{-6}}{1.73}}{\frac{1.5549 \cdot \mathrm{e}^{-6}}{0.1}} = 0.2519$$

Analytical results in comparison with numerical results for longitudinal tension

Figure 5. represents analytical results from compcomp in comparison with the result from Calculix. As was expected lower bounds are identical with Mori-Tanaka estimates and numerical result lies in the bounds range. That indicates correct results..

The difference between lower and upper bounds is for longitudinal elastic modulus very small and in whole fiber volume scale almost identical, therefore zoomed scale was chosen to show results adequately.

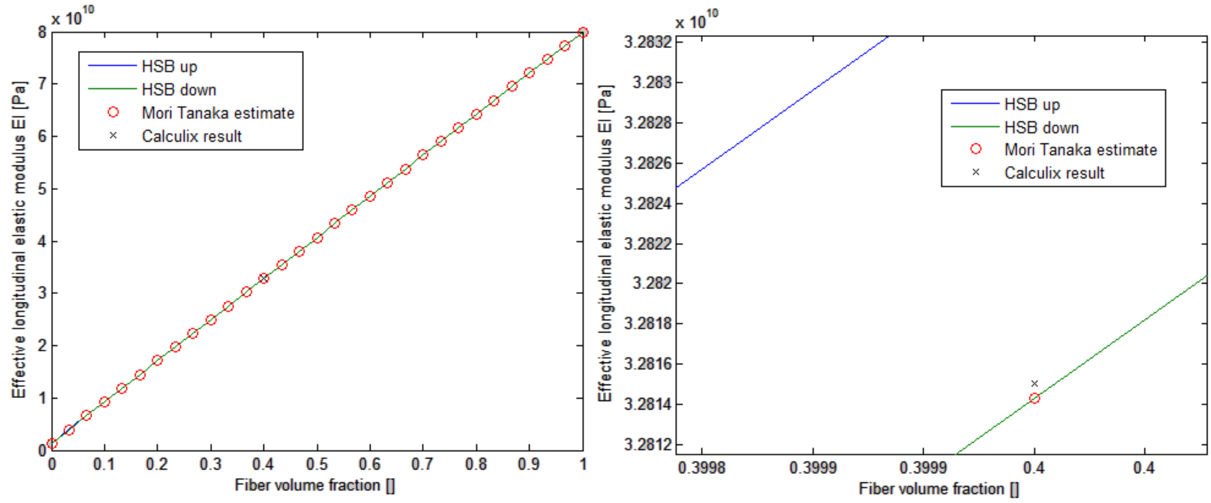

Fig. 5. Comparison of the analytical and numerical results for longitudinal tension

Analytical results in comparison with numerical results for longitudinal poisson ratio

Figure 6. represents analytical results from compcomp in comparison with the result from Calculix. Upper bounds are identical with Mori-Tanaka estimates and numerical result lies in the bounds range. That indicates correct results.

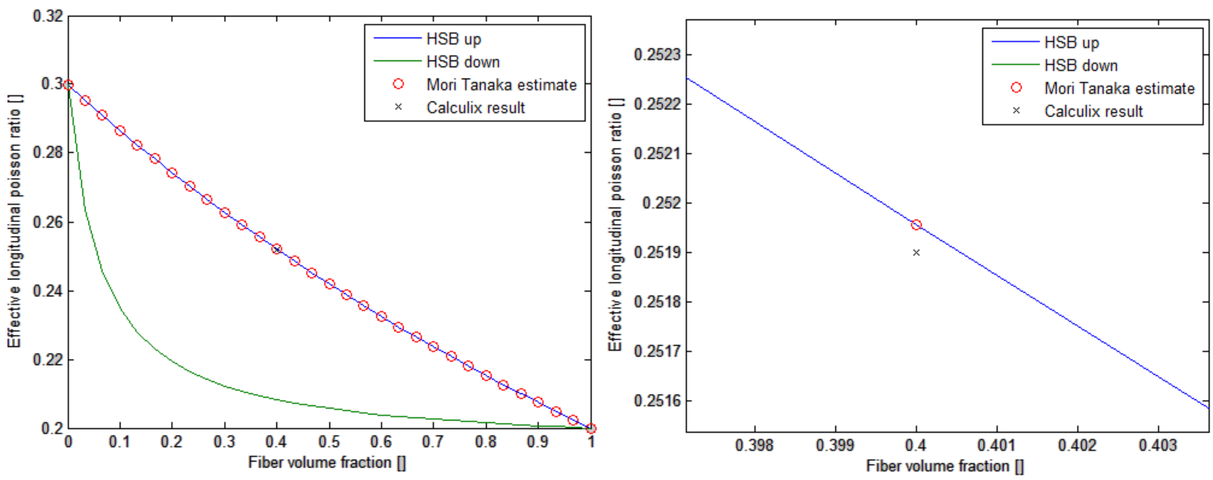

Fig. 6. Comparison of the analytical and numerical results for longitudinal poisson ratio

Unit cell deformation for longitudinal tension

On the figure 7. are displayed deformed and undeformed shape of the unit cell for longitudinal tension.

Applied force in longitudinal direction extends the unit cell and the contraction in the transverse direction and in the direction normal to the transverse direction is caused by poisson effect.

Shape of the unit cell is block after the deformation so the periodic and symmetry boundary conditions are fulfilled.

Deformed shape is scaled with factor of 100 000 to make the deformation visible.

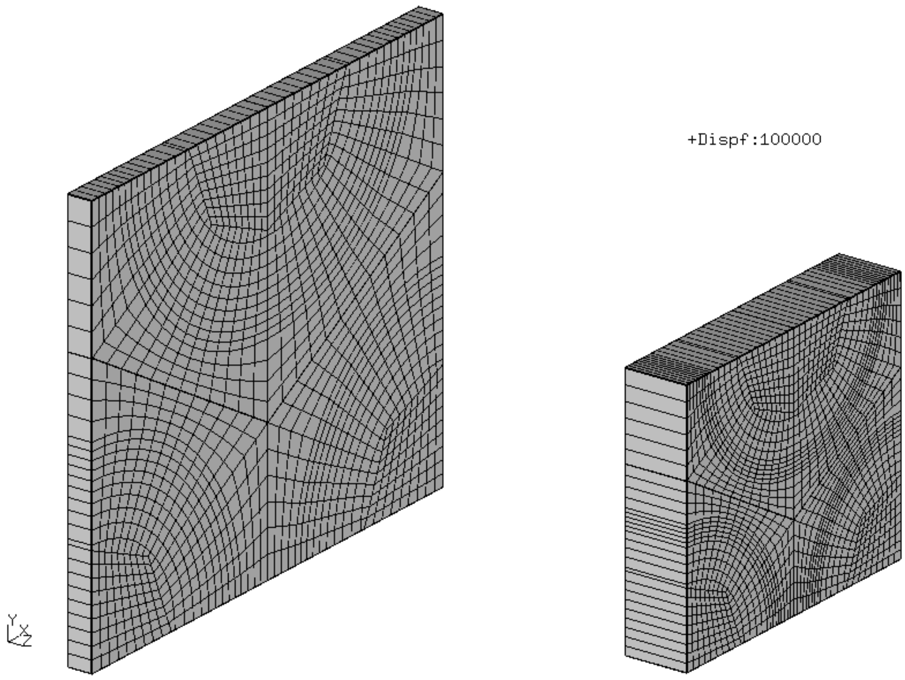

Fig. 7. Unit cell deformation for longitudinal tension

Mean field stress in comparison with micro field stresses for longitudinal tension

On the figure 8. are shown micro stress fields σ_{ll} and σ_{tq}. Due to the periodic boundary condition and boundary conditions that represent longitudinal tension have to be fibers and matrix deformed by equal length.

Since the matrix has lower Young's modulus than fibers, resulting stresses are higher in fibers and lower in matrix. Mentioned boundary conditions and differences in Young's modulus of the fibers and matrix causes also shear stresses in the unit cell

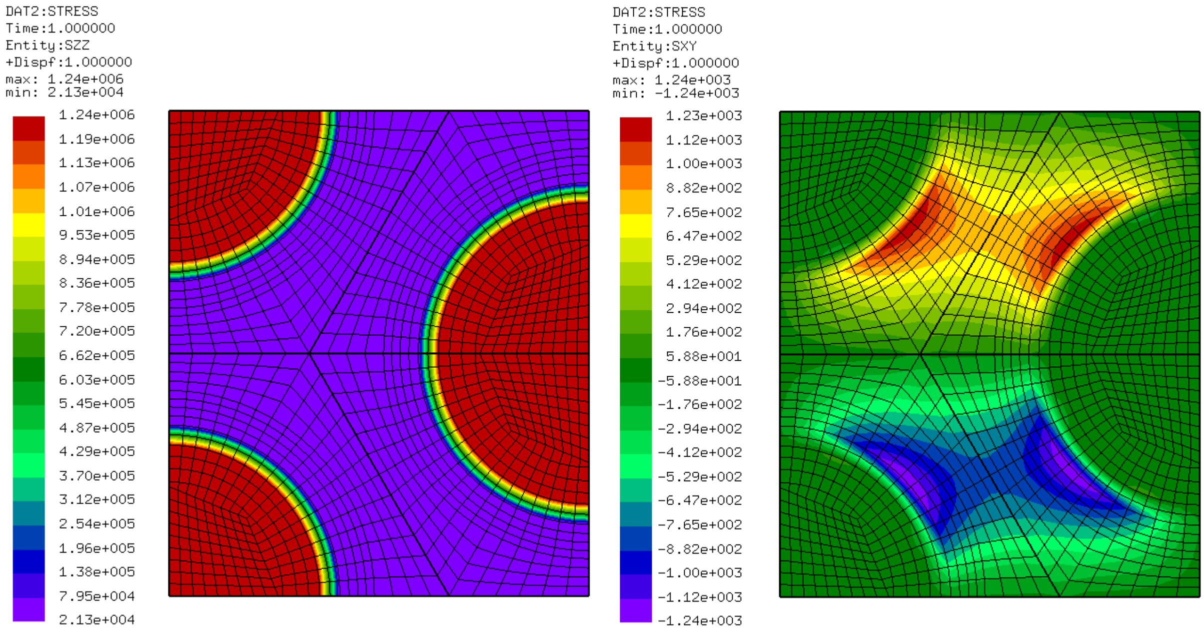

Fig. 8. Micro field stresses for longitudinal tension σ_{ll} (left), σ_{tq}(right)

Figure 9. represents the micro field stresses σ_{tt} and σ_{qq}. Poisson effect boundary conditions and differences in stiffness of the matrix and the fibers causes stress distribution where fibers are compressed and matrix tensed.

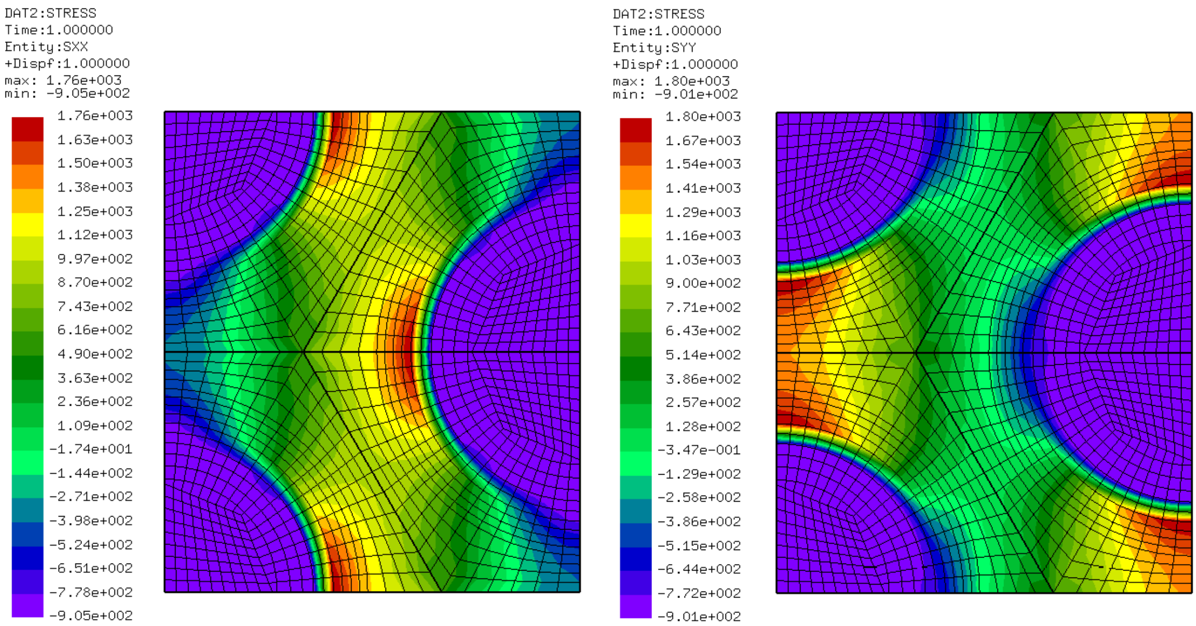

Fig. 9. Micro field stresses for longitudinal tension σ_{tt} (left), σ_{qq}(right)

Mean stress in longitudinal direction is $\sigma_{ll} = 5.1023 \cdot \mathrm{e}^5 Pa$. I comparison with the stress range by micro field stress is visible the effect of the homogenization.

Transverse tension

Boundary conditions for master nodes are showed in the figure 10.

Corresponding modulus	Master nodes	x-displacement [m]	y-displacement [m]	z-displacement [m]
E_t	1 (0,0,0)	FIXED	FIXED	FIXED
	1348 (0, 1.73,0)	FIXED	FREE	FIXED
	2001 (2,0,0)	LOAD	FIXED	FIXED
	10001 (0,0, 0.1)	FREE	FREE	FREE

Fig. 10. Boundary conditions for transverse tension

Master nodes displacements are showed in the figure 11.:

Corresponding modulus	Master nodes	x-displacement [m]	y-displacement [m]	z-displacement [m]
E_t	1 (0,0,0)	0	0	0
	1348 (0, 1.73,0)	0	-2.3386e-03	0
	2001 (2,0,0)	6.9503e-03	0	0
	10001 (0,0, 0.1)	0	0	-7.8347e-06

Fig. 11. Master nodes displacements for transverse tension

Computation of the transverse tension modulus:

$$\frac{F}{c \cdot b} = E_t \cdot \frac{x_{2001}}{a} \rightarrow E_t = \frac{a \cdot F}{c \cdot b \cdot x_{2001}} = \frac{2 \cdot 1{,}7675 \cdot e^{6}}{0.1 \cdot 1.73 \cdot 6.9503 \cdot \mathrm{e}^{-3}} = 2.9365 \cdot \mathrm{e}^{9}\ Pa$$

Computation of the transverse poisson ratio:

$$\nu_{qt} = -\frac{\varepsilon_{qq}}{\varepsilon_{tt}} = \frac{\frac{y_{1348}}{b}}{\frac{x_{2001}}{a}} = -\frac{\frac{-2.3385 \cdot \mathrm{e}^{-3}}{1.73}}{\frac{6.9503 \cdot \mathrm{e}^{-3}}{2}} = \ 0.3885$$

Analytical results in comparison with numerical results for transverse tension

Figure 12. represents analytical results from compcomp in comparison with the result from Calculix. Lower bounds are identical with Mori-Tanaka estimates and numerical result lies in bounds range. That indicates correct results..

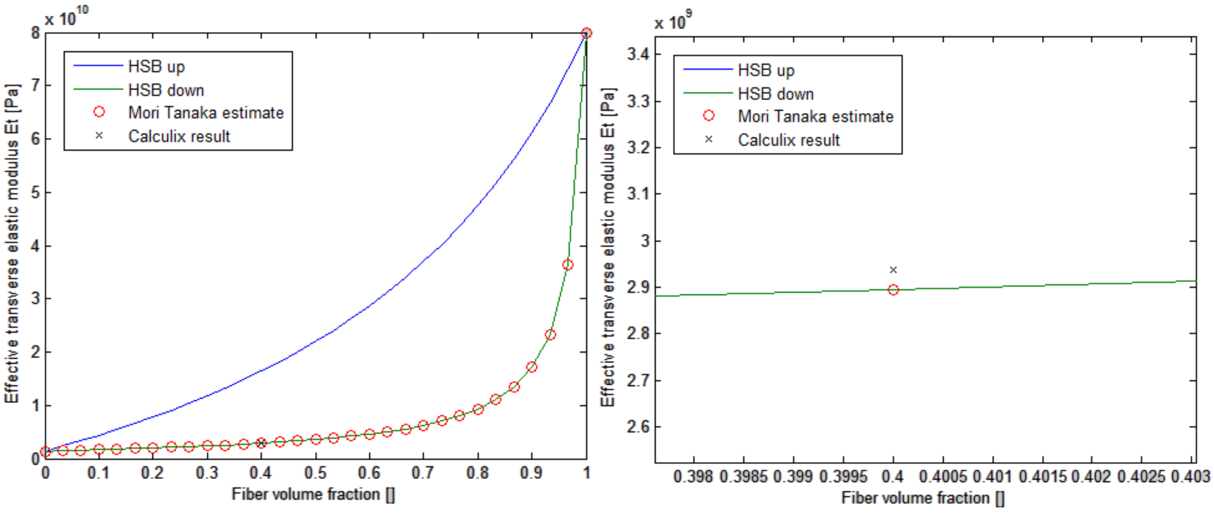

Fig. 12. Comparison of the analytical and numerical results for transverse tension

Analytical results in comparison with numerical results for transverse poisson ratio

Figure 13. represents analytical results from compcomp in comparison with the result from Calculix. Lower bound is negative and the upper bound in not identical with the Mori-Tanaka estimate. Results were double checked but no mistake during obtaining the results from comcomp was noticed.

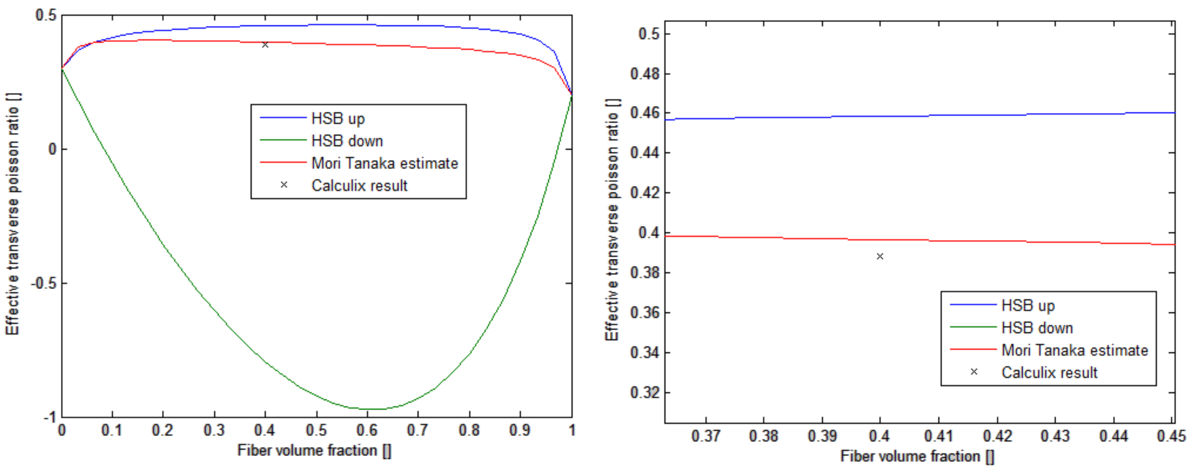

Fig. 13. Comparison of the analytical and numerical results for transverse poisson ratio

Unit cell deformation for transverse tension

On the figure 14. are displayed deformed and undeformed shape of the unit cell for transverse tension.

Similar to the longitudinal tension the deformed shape of the unit cell is a block. Unit cell is extended in the transverse direction and compressed in longitudinal direction as well as in the direction normal to transverse direction.

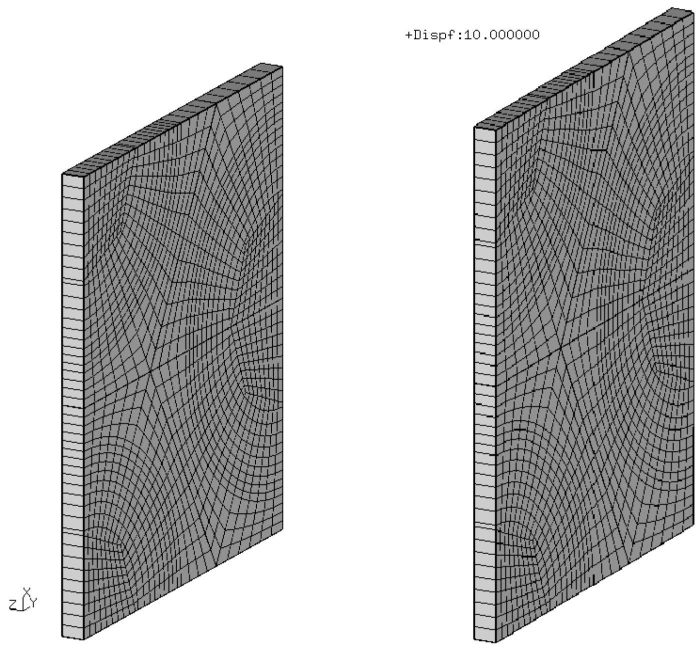

Fig. 14. Unit cell deformation for longitudinal tension

Mean field stress in comparison with micro field stresses for transverse tension

On the figure 15. are shown micro stress field σ_{tt} and σ_{qq}.Stress field σ_{tt} is in the direction of the loading. As before matrix has lower Young's modulus than fibers therefore higher stresses are in the fibers.

Stress field σ_{qq} is caused by poisson effect. Contraction causes compressive but also tensile components of micro-field in the areas where material properties are changing.

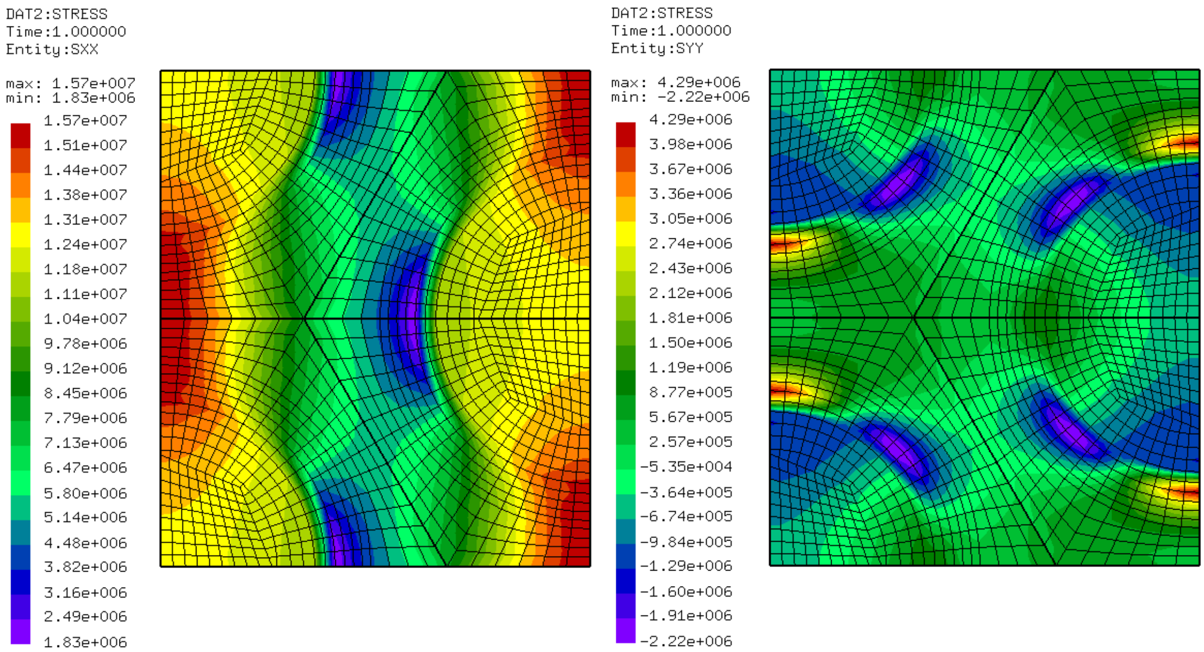

Fig. 15. σ_{tt} (left), σ_{qq} (right) for transverse tension

On the figure 16. are shown stress field σ_{ll} and σ_{tq}.Stress field σ_{ll} is also caused by the poisson effect. High Young's modulus of the fibers causes compressive stresses in fibers and lower Young's modulus of the matrix causes tensile stresses in matrix.

Interesting are the shear stresses σ_{tq}. Their intensity is high at the material borders

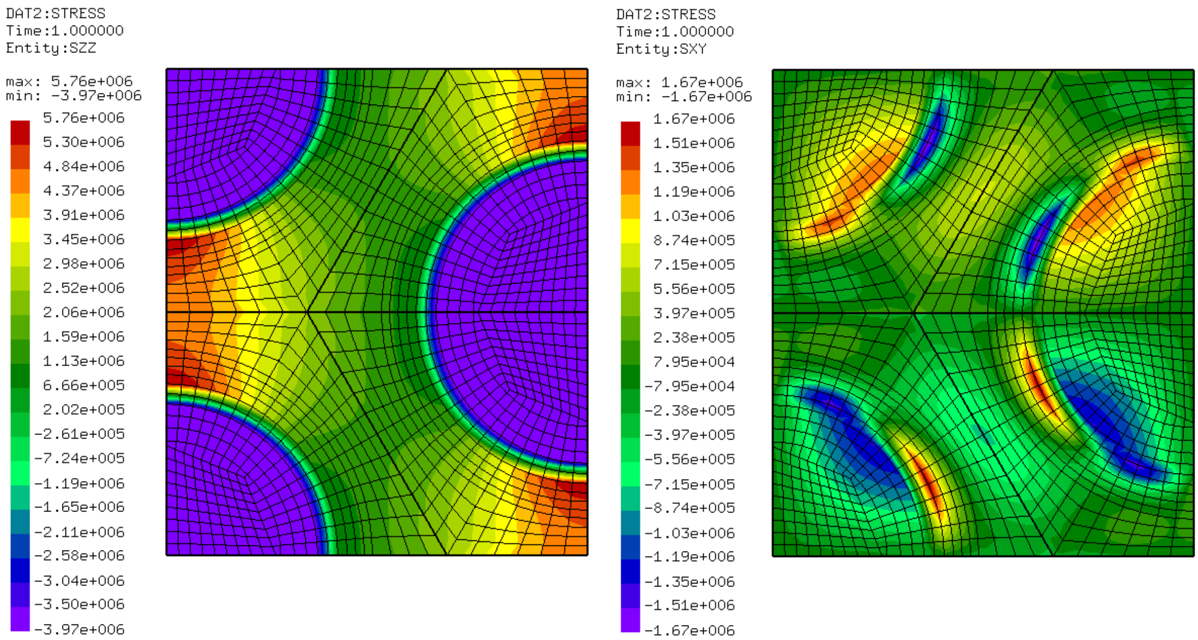

Fig. 16. σ_{ll} (left), σ_{tq} (right) for transverse tension

Mean stress for transverse tension is $\sigma_{tt} = 1.0205 \cdot e^7\ Pa$

Longitudinal shear

Boundary conditions for master nodes are showed in the figure 17.

Corresponding modulus	**Master nodes**	**x-displacement [m]**	**y-displacement [m]**	**z-displacement [m]**
G_{lt}	1 (0,0,0)	FIXED	FIXED	FIXED
	1348 (0, 1.73,0)	FIXED	FIXED	FIXED
	2001 (2,0,0)	FIXED	FIXED	LOAD
	10001 (0,0, 0.1)	FREE	FREE	FIXED

Fig. 17. Boundary conditions for longitudinal shear

Master nodes displacements are showed in the figure 18.:

Corresponding modulus	**Master nodes**	**x-displacement [m]**	**y-displacement [m]**	**z-displacement [m]**
G_{lt}	1 (0,0,0)	0	0	0
	1348 (0, 1.73,0)	0	0	0
	2001 (2,0,0)	0	0	1.7327e-02
	10001 (0,0, 0.1)	0	0	0

Fig. 18. Master nodes displacements for longitudinal shear

Computation of the longitudinal shear modulus:

$$\frac{F}{c \cdot b} = G_{lt} \cdot \frac{z_{2001}}{a} \rightarrow G_{lt} = \frac{a \cdot F}{c \cdot b \cdot z_{2001}} = \frac{2 \cdot 1{,}7675 \cdot e^{6}}{0.1 \cdot 1.73 \cdot 1.7327 \cdot \mathrm{e}^{-2}} = 1.1779 \cdot \mathrm{e}^{9}\ Pa$$

Analytical results in comparison with numerical results for longitudinal shear

Figure 19. represents analytical results from compcomp in comparison with the result from Calculix. Lower bounds are identical with Mori-Tanaka estimates and numerical result lies in the bounds range. That indicates correct results.

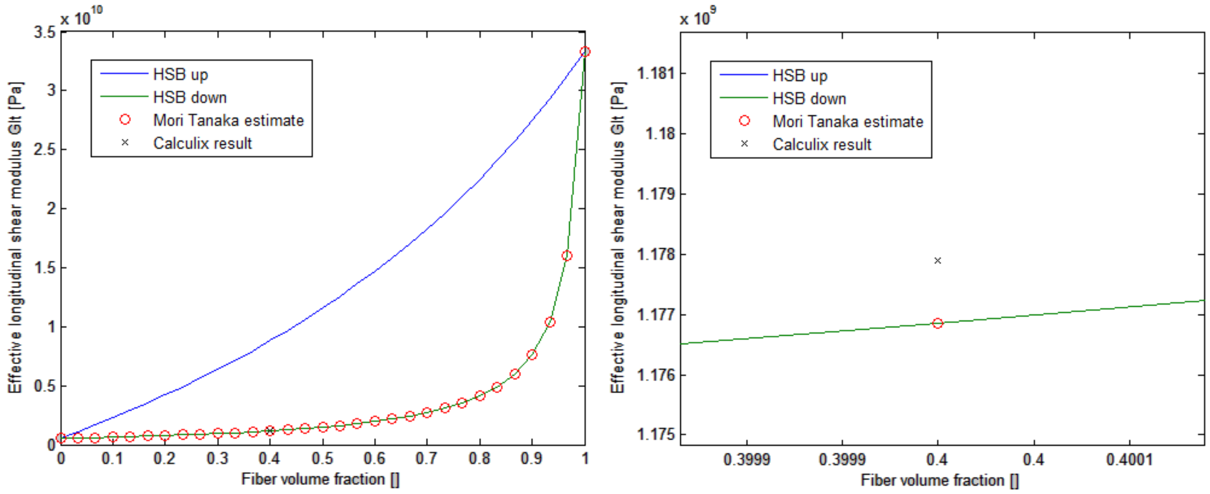

Fig. 19. Comparison of the analytical and numerical results for longitudinal shear

Unit cell deformation for longitudinal shear

On the figure 20. are displayed deformed and undeformed shape of the unit cell for longitudinal shear.

For longitudinal shear load case are the periodic boundary conditions easier to see. Their fulfillment is represented by colorful lines in the figure 20.

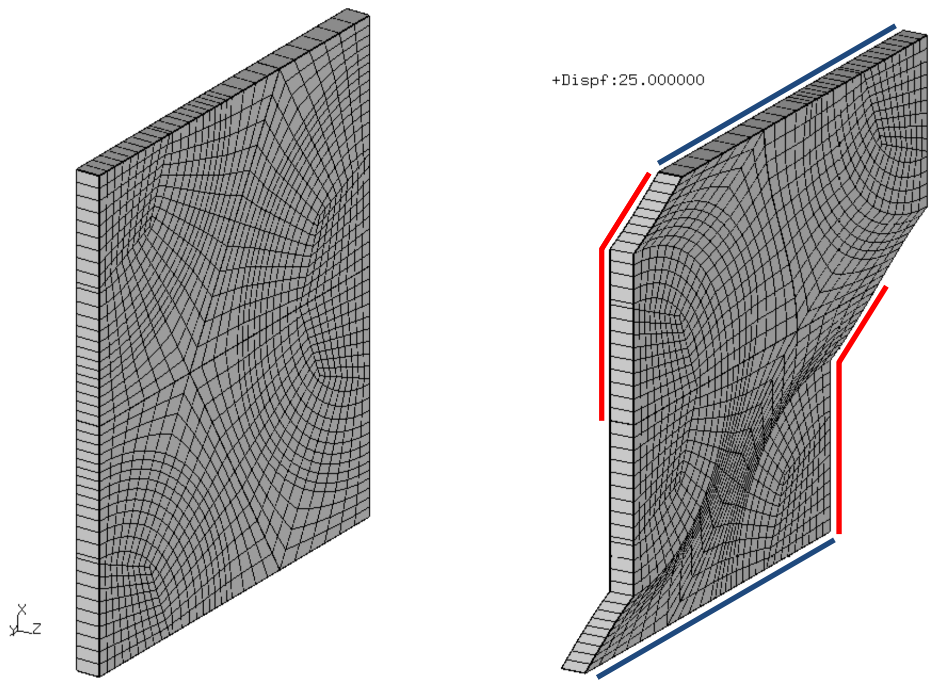

Fig. 20. Unit cell deformation for longitudinal shear

Mean field stress in comparison with micro field stresses for longitudinal shear.

On the figure 21. is shown the stress field σ_{lt}. Stress field σ_{lt} shows higher shear stress components in the fibers

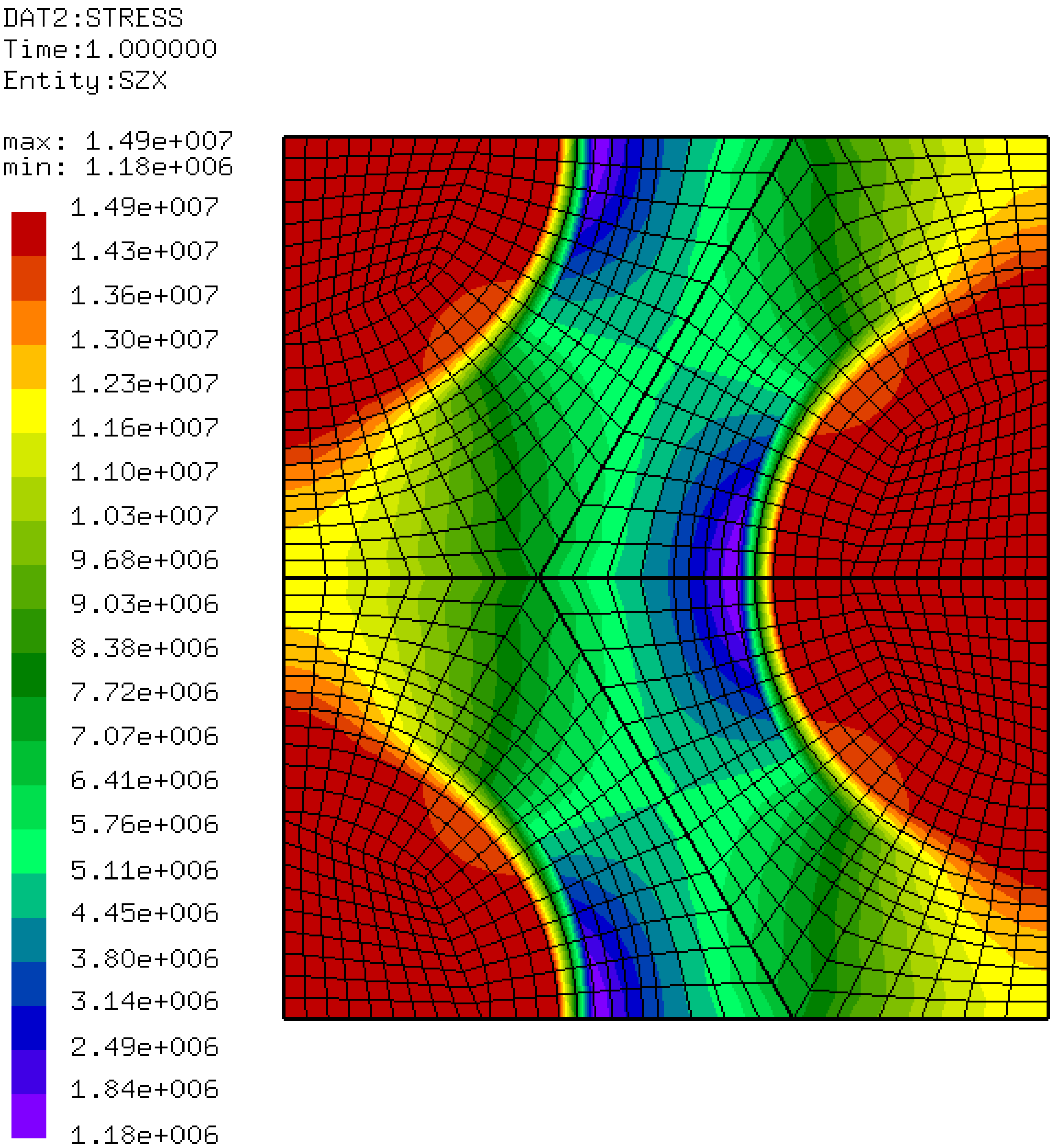

Fig. 21. Stress field σ_{lt} for longitudinal shear.

Mean stress for longitudinal shear is $\sigma_{lt} = 1.0205 \cdot e^{7}\ Pa$.

Transverse shear

Boundary conditions for master nodes are showed in the figure 22.

Corresponding modulus	Master nodes	x-displacement [m]	y-displacement [m]	z-displacement [m]
G_{tq}	1 (0,0,0)	FIXED	FIXED	FIXED
	1348 (0, 1.73,0)	FIXED	FIXED	FIXED
	2001 (2,0,0)	FIXED	LOAD	FIXED
	10001 (0,0, 0.1)	FREE	FREE	FIXED

Fig.22. Boundary conditions for transverse shear

Master nodes displacements are showed in the figure 23.:

Corresponding modulus	Master nodes	x-displacement [m]	y-displacement [m]	z-displacement [m]
G_{tq}	1 (0,0,0)	0	0	0
	1348 (0, 1.73,0)	0	0	0
	2001 (2,0,0)	0	1.9301e-02	0
	10001 (0,0, 0.1)	0	0	0

Fig.23. Master nodes displacements for transverse shear

Computation of the transverse shear modulus:

$$\frac{F}{c \cdot b} = G_{tq} \cdot \frac{y_{2001}}{a} \rightarrow G_{tq} = \frac{a \cdot F}{c \cdot b \cdot y_{2001}} = \frac{2 \cdot 1{,}7675 \cdot e^{6}}{0.1 \cdot 1.73 \cdot 1.9301 \cdot \mathrm{e}^{-3}} = 1.0574 \cdot \mathrm{e}^{9}\ Pa$$

Analytical results in comparison with numerical results for transverse shear

Figure 24. represents analytical results from compcomp in comparison with the result from Calculix. Lower bounds are identical with Mori-Tanaka estimates and numerical result lies in the bounds range. That indicates correct results.

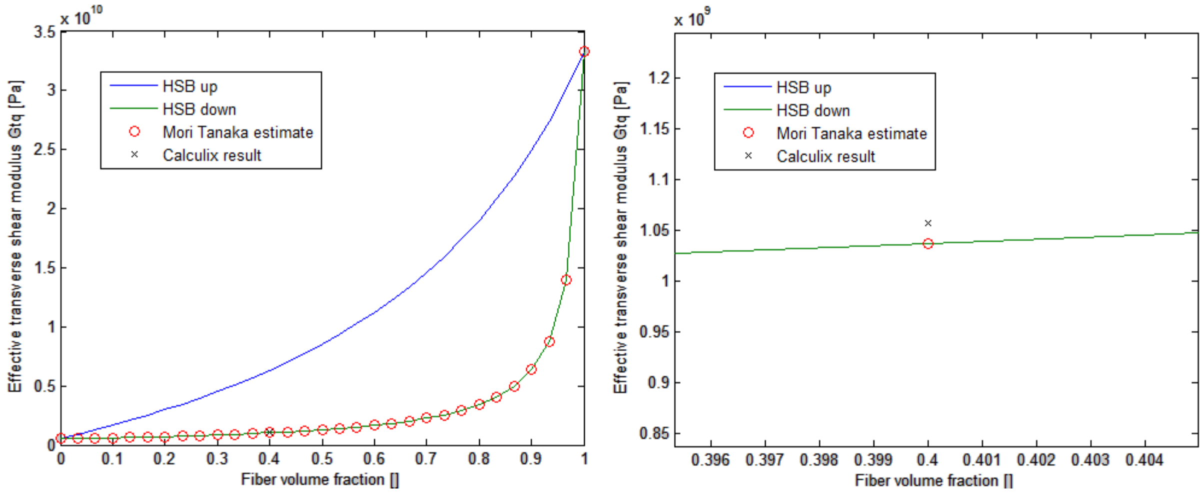

Fig. 24. Comparison of the analytical and numerical results for transverse shear

Unit cell deformation for transverse shear

On the figure 25. are displayed deformed and undeformed shape of the unit cell for transverse shear.

Figure shows that most of the deformation is performed on the matrix due to lower stiffness and the fibers remain almost undeformed.

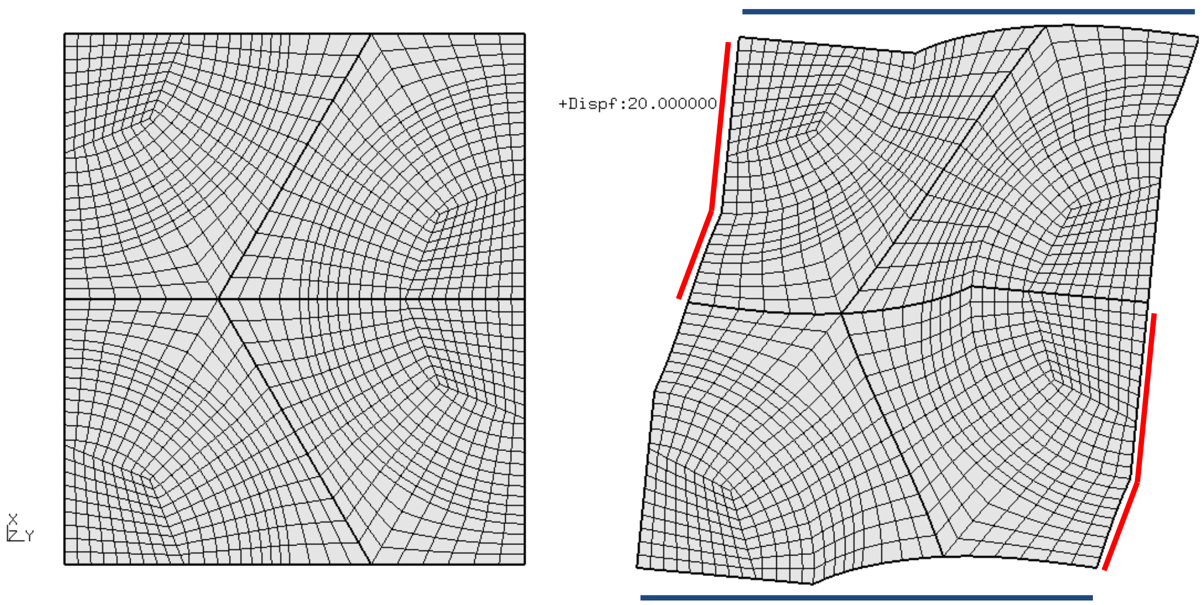

Fig. 25. Unit cell deformation for transverse shear

Mean field stress in comparison with micro field stresses for transverse shear.

On the figure 26. is shown stress field σ_{tq}. Stress field σ_{tq} shows that "stress belt" of higher stress value is passing vertically between the fibers and has a peak value at the contact with the fiber.

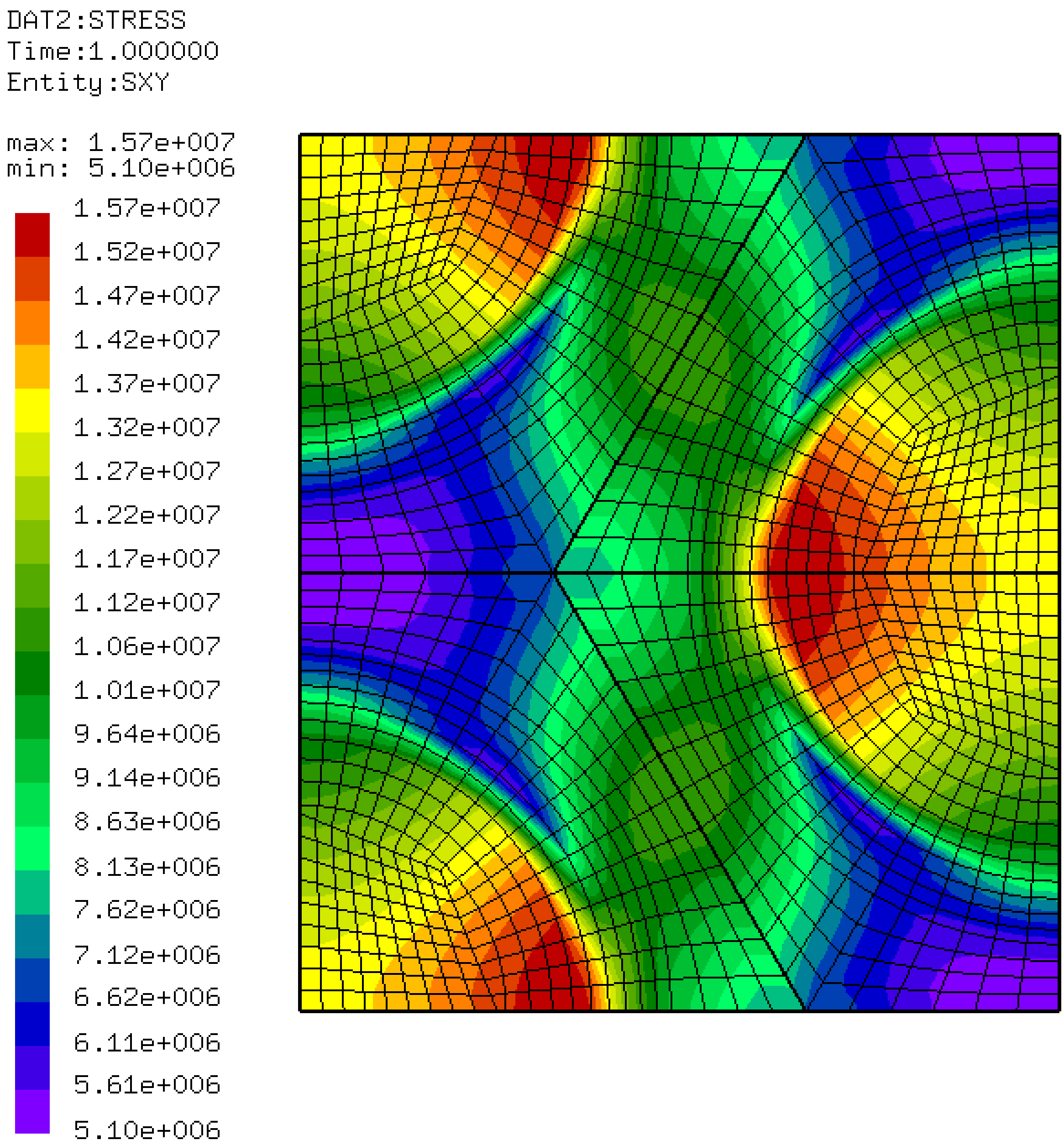

Fig. 26. Stress field σ_{tq} for transverse shear

Mean stress for transverse shear is $\sigma_{lt} = 1.0205 \cdot e^{7}\ Pa$.

Coefficients of thermal expansion

The temperature difference was set to *1K* for computational purposes.

Boundary conditions for master nodes are showed in the figure 27.

Corresponding CTE	**Master nodes**	**x-displacement [m]**	**y-displacement [m]**	**z-displacement [m]**
$\boldsymbol{\alpha_l, \alpha_t}$	1 (0,0,0)	FIXED	FIXED	FIXED
	1348 (0, 1.73,0)	FREE	FREE	FIXED
	2001 (2,0,0)	FREE	FIXED	FIXED
	10001 (0,0, 0.1)	FREE	FREE	FREE

Fig. 27. Boundary conditions for the coefficients of the thermal expansion

Master nodes displacements are showed in the figure 28.:

Corresponding CTE	**Master nodes**	**x-displacement [m]**	**y-displacement [m]**	**z-displacement [m]**
$\boldsymbol{\alpha_l, \alpha_t}$	1 (0,0,0)	0	0	0
	1348 (0, 1.73,0)	0	1.5333e-04	0
	2001 (2,0,0)	1.7706e-04	0	0
	10001 (0,0, 0.1)	0	0	8.2006e-07

Fig. 28. Master nodes displacements for the **c**oefficients of the thermal expansion

General equation for CTE computation:

$$\varepsilon_{th} = \alpha \cdot \left(T - T_{ref}\right) \rightarrow \frac{\Delta l}{l} = \alpha \cdot \left(T - T_{ref}\right) \rightarrow \alpha = \frac{\Delta l}{l \cdot \left(T - T_{ref}\right)}$$

Computation of the longitudinal CTE:

$$\alpha_l = \frac{z_{10001}}{c \cdot \left(T - T_{ref}\right)} = \frac{8.2006 \cdot e^{-7}}{0.1 \cdot (274 - 273)} = 8.2006 \cdot e^{-6} K^{-1}$$

Computation of the transverse CTE:

$$\alpha_t = \alpha_q = \frac{x_{2001}}{a \cdot \left(T - T_{ref}\right)} = \frac{y_{1348}}{b \cdot \left(T - T_{ref}\right)} = \frac{1.7706 \cdot e^{-4}}{2 \cdot 1} = \frac{1.5333 \cdot e^{-4}}{1.73 \cdot 1} = 8.85 \cdot e^{-5} K^{-1}$$

Analytical results in comparison with numerical results for thermal load cases

Figure 29. represents analytical results from compcomp in comparison with the result from Calculix. Compcomp did not provide results for CTE values of the bounds therefore only Mori-Tanaka estimates are displayed. Assuming that the lower bound is identical with Mori- Tanaka estimates for longitudinal CTE, than numerical results lies in the bounds range and that indicates correct result

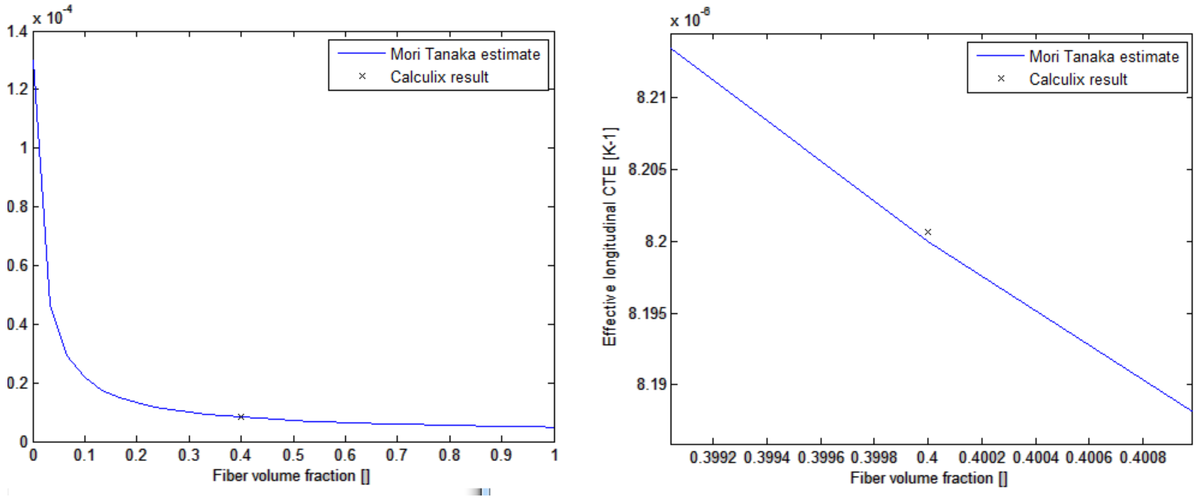

Fig. 29. Comparison of the analytical and numerical results longitudinal CTE

Figure 30. represents analytical results from compcomp in comparison with the result from Calculix. Compcomp did not provide results for CTE values of the bounds therefore only Mori-Tanaka estimates are displayed. Assuming that the higher bound is identical with Mori- Tanaka estimates for transverse CTE, than numerical results lies in the bounds range and that indicates correct result

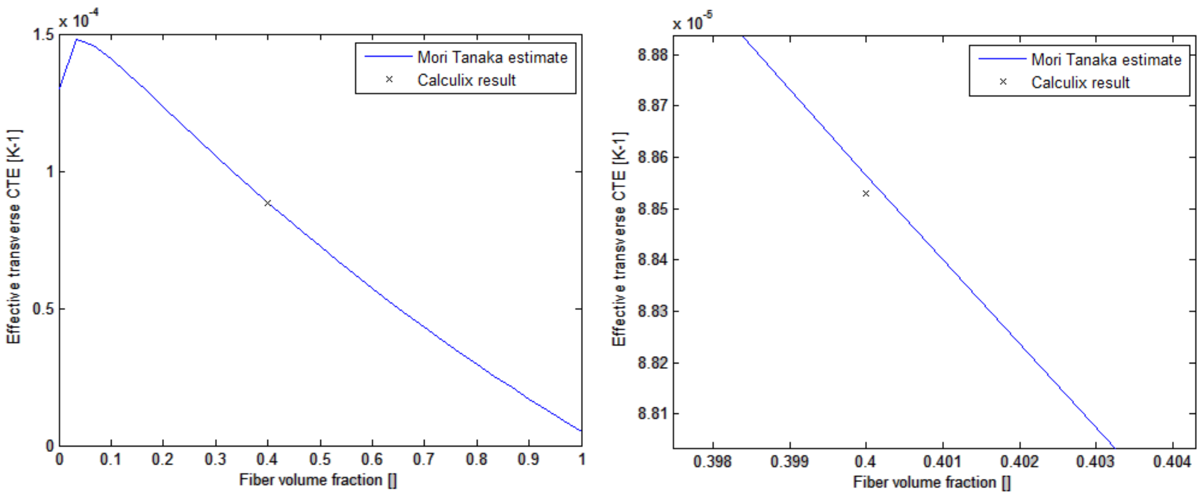

Fig. 30. Comparison of the analytical and numerical results longitudinal CTE

Unit cell deformation for thermal loading

On the figure 31. are displayed deformed and undeformed shape of the unit cell for thermal load case.

Figure shows that the unit cell is expanded in all directions

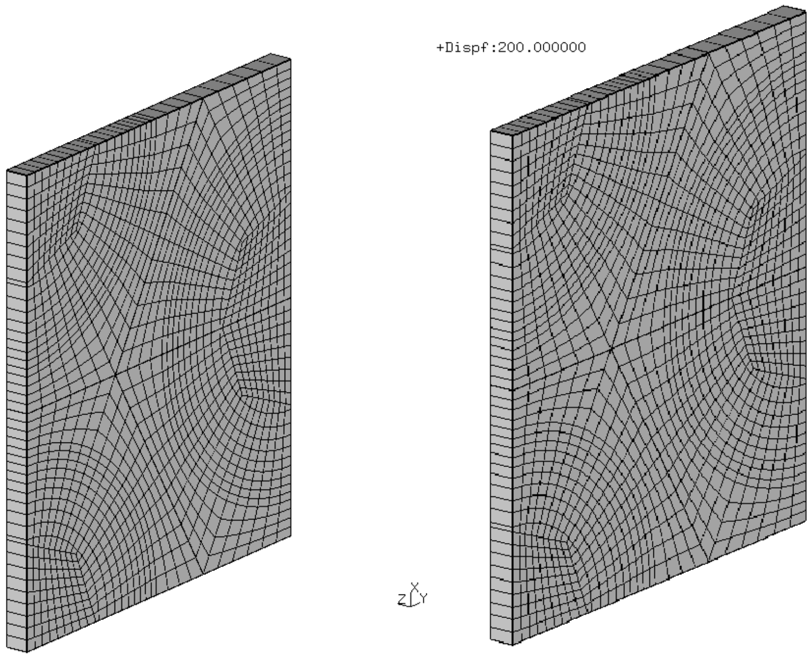

Fig. 31. Unit cell deformation for thermal load case

Mean field stress in comparison with micro field stresses for thermal load case

On the figure 34. are shown micro stress field σ_{tt} and σ_{qq}.Matrix has the CTE much higher than fibers also the arrangement of boundary conditions of master nodes and the difference in the stiffness causes that fibers are under higher stress than the matrix is. There are also locations where in the matrix compressed.

Figure 35.shows Von Mises equivalent stresses and σ_{ll}

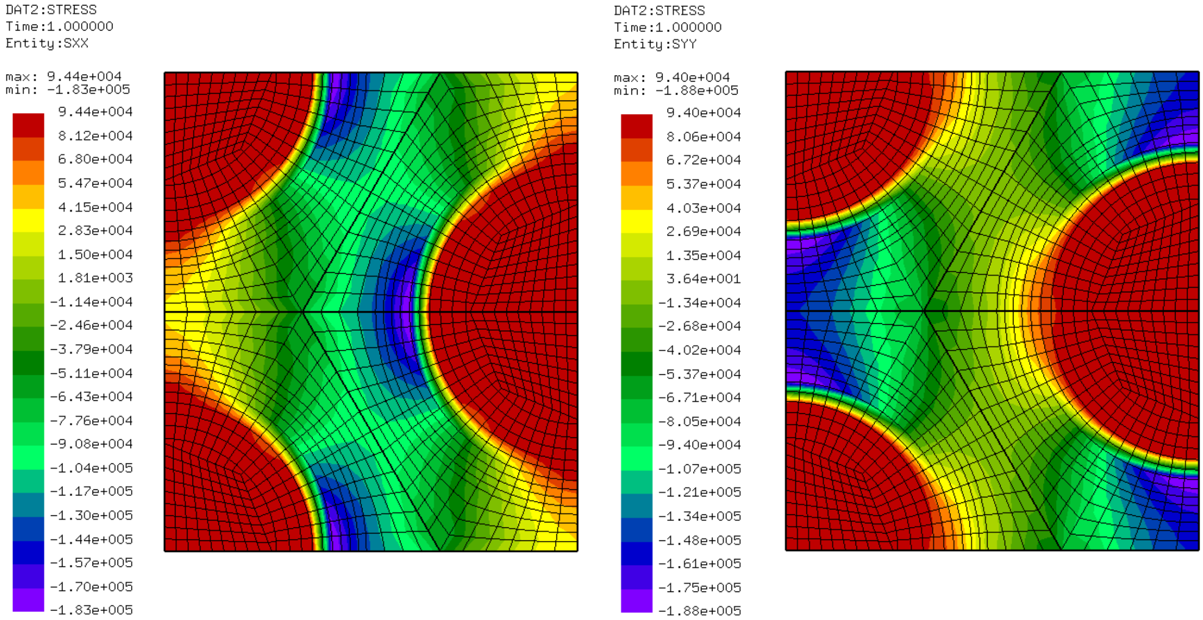

Fig. 34. σ_{tt} (left), σ_{qq} (right) for thermal load case

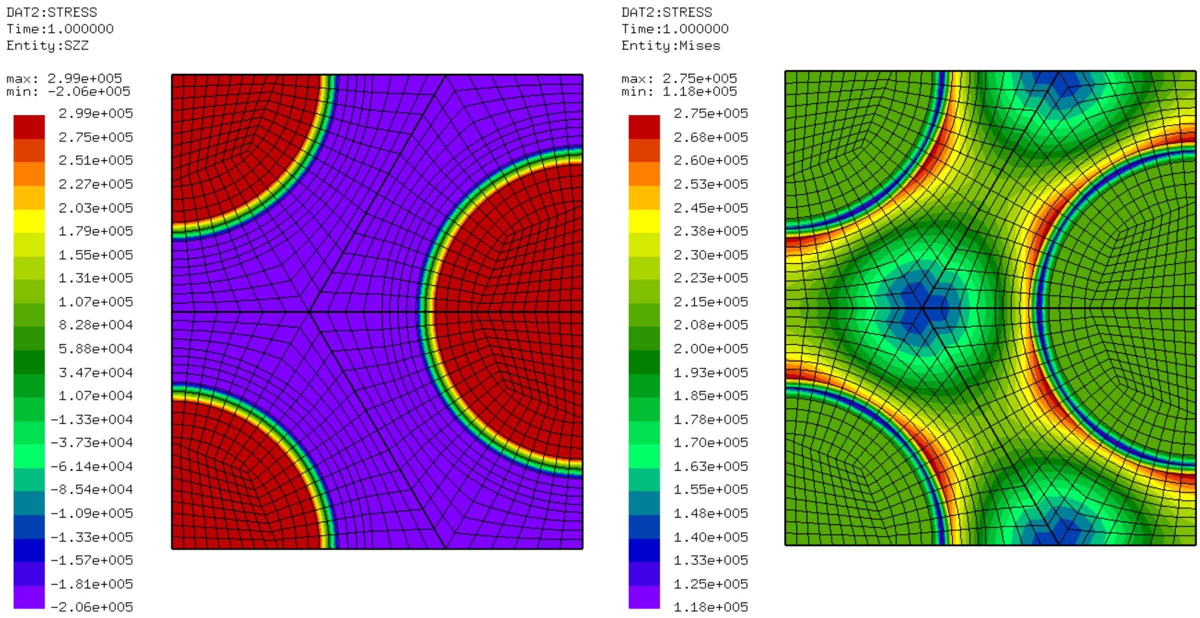

Fig. 35. σ_{ll} (left), Von Mises (right) for thermal load case

Summary

Sufficient number of material properties to describe transverse isotropic material were calculated by numerical approach and compared to results from analytical approach.

Numerical results matched the analytical results in all load cases satisfyingly with respect to the position in the range of the Hashin-Shtrikman bounds. Periodic and symmetry boundary conditions as well as the micro stress field were discussed.

Problems have occurred by analytical results for transverse poisson ratio where lower bounds were negative and upper bounds did not match the Mori-Tanaka estimates. Despite this problem was the numerical results close to Mori-Tanaka estimate.